Folded potential analysis of the excitation of giant resonances by heavy ions

D. J. Horen,* J. R. Beene, and G. R. Satchler
Oak Ridge National Laboratory, Oak Ridge, Tennessee 37831
(Received 17 May 1995)

Measurements of the excitation of nuclear giant resonances by heavy-ion inelastic scattering have previously been analyzed using the deformed optical potential model. Here we reexamine these data using a folded potential model which employs a simple, but effective, nucleon-nucleon interaction that was deduced recently from heavy-ion elastic scattering measurements. The resulting estimates of the sum-rule exhaustion by the giant quadrupole resonance increase by amounts ranging from about 20% for the lighter targets to no change for ^{208}Pb. Applying the same model to data for excitation of the giant monopole resonance, we find that these transitions overexhaust the corresponding sum rule even more than previously indicated.

PACS number(s): 24.30.Cz, 24.10,−i, 25.70.Bc

I. INTRODUCTION

There are advantages to the excitation of nuclear giant multipole resonances by the inelastic scattering of heavy ions with intermediate energies [1,2]. In particular, a number of recent experiments have employed beams of ^{17}O ions at $E/A = 84$ MeV [3–7]. We concentrate our attention on these because they provide the most complete results on giant resonance excitation.

The deformed optical potential (DP) model [8,9] has been the primary tool for the analysis of these measurements. However, it has long been known that the DP model may give results differing significantly from a more microscopic approach in which a transition potential is obtained by folding an effective nucleon-nucleon interaction over the target transition density and the projectile ground-state density. We take the view that the transition density and its properties are the quantities of interest, characteristic of a given target nucleus, that we wish to deduce from measured cross sections. The folding procedure provides a direct link between the transition density and the corresponding transition potential for a particular projectile ion that is responsible for the observed inelastic scattering. This link is left ambiguous and obscure by use of the DP model. This situation has been reexamined recently [10]. In particular, applications of the folding and DP models to the excitation of low states by ^{17}O ions with $E/A = 84$ MeV have been compared [11], and an apparent hindrance in the hadronic excitation of 3^- states [7], compared to electromagnetic measurements, could be ascribed to the use of the DP model. The "hindrance" is removed when the folding model is used [11]. The apparent discrepancy was not small, being typically a factor of order 2.

The differences between folding and the DP model that are found for the excitation of low 2^+ states are somewhat smaller [11], especially for transitions in which Coulomb excitation is very important, but nonetheless they can be significant. Consequently one may ask how a folding approach will affect our estimate of the fraction of the sum-rule limit [8,9] that is exhausted by excitation of a giant quadrupole resonance (GQR). Furthermore, there has been a long-standing disagreement over the interpretation of these transitions as induced by pion inelastic scattering compared to the use of other hadrons, especially heavy ions [12]. This disagreement translates into very different conclusions about the isospin character of the GQR. The heavy-ion data have previously been analyzed using the DP model; we show here that the folding model approach does not change this disagreement significantly.

The choice of a DP model to generate a transition potential for the excitation of a giant monopole ("breathing mode") resonance (GMR) is particularly ambiguous, especially for heavy ions. Here again the folding procedure provides a direct link between the potential and the underlying transition density. Hence we have also applied folding to GMR transitions.

II. THE MODELS

The simple models chosen for use here for illustration are standard ones, and we follow the notation of Ref. [9].

A. Folded transition potential

In the folding procedure, the transition potential can be written as [8]

$$G^F_\ell(r) = \int g_{T\ell}(r_T)\bar{v}_\ell(r,r_T)r_T^2 dr_T, \tag{2.1}$$

where $g_{T\ell}(r)$ is the transition density for a 2^ℓ-pole excitation of the target and $\bar{v}_\ell(r,r_T)$ is the 2^ℓ-pole component of an effective nucleon-nucleon interaction $v(s)$ averaged over the (spherical) projectile density distribution $\rho_p(r')$. The integral (2.1) is most simply expressed and evaluated in terms of Fourier transforms [13]

$$G^F_\ell(r) = (2\pi^2)^{-1}\int k^2 dk j_\ell(kr)\tilde{v}(k)\tilde{g}_{T\ell}(k)\tilde{\rho}_p(k), \tag{2.2}$$

where $\tilde{f}(k)$ is the Fourier transform of $f(r)$. For $v(s)$, we take the isoscalar Yukawa form

*Present address: Department of Physics, University of Connecticut, Storrs, CT 06269.

TABLE I. Density distribution parameters and sum-rule limits for giant quadrupole resonances with excitation energy E_x.

Target	E_x (MeV)	c (fm)	a (fm)	$\langle r^2\rangle_m^{1/2}$ (fm)	B(IS,2) (b^2)	$B(E2)$ (e^2 b^2)	δ_2^m (fm)	α_2^m
^{60}Ni	16.0	4.20	0.475	3.702	0.427	0.093	0.971	0.200
^{90}Zr	14.0	4.90	0.515	4.251	0.966	0.191	0.846	0.152
^{118}Sn	12.8	5.52	0.515	4.685	1.683	0.302	0.771	0.126
^{120}Sn	13.1	5.55	0.515	4.706	1.687	0.293	0.755	0.123
^{124}Sn	12.5	5.62	0.515	4.756	1.866	0.303	0.761	0.122
^{208}Pb	10.6	6.67	0.545	5.550	5.026	0.781	0.636	0.088

$$v(s)=-(v+i\omega)\frac{e^{-s/t}}{s/t} \tag{2.3}$$

with $t=0.7$ fm, recently found to give a good account of heavy-ion elastic scattering in peripheral collisions. The strengths v and w were obtained by fitting the elastic data [14].

We note that the shape of the folded transition potential (2.1) depends upon ℓ, through the ℓ dependence of $\bar{v}_\ell$, even if the transition density has a shape that is independent of ℓ [11]. This arises because of the finite range of $v(s)$ and the finite size of the projectile [10,15].

B. Transition densities

The transition density $g_\ell(r)$ needed for the folding (2.1) or (2.2) may be constructed using a simple model or from detailed nuclear structure calculations. For our purpose, we adopt the Bohr-Mottelson (BM) [16] model, namely,

$$g_\ell^{\rm BM}(r)=-\delta_\ell^m d\rho(r)/dr \tag{2.4}$$

for $\ell\geq 2$, where $\rho(r)$ is the ground-state density distribution of the target nucleus and δ_ℓ^m is the deformation length which provides a measure of the strength of the transition. We take the breathing mode form [17] for the GMR

$$g_0(r)=-\alpha_0^m[3\rho(r)+r d\rho(r)/dr]. \tag{2.5}$$

The ground-state densities are represented by two-parameter Fermi (or Woods-Saxon) functions

$$\rho(r)=\rho_0\{1+\exp[(r-c)/a]\}^{-1}. \tag{2.6}$$

The chosen parameter values, indicated in Table I, are the same as those used in [14] to fit the elastic scattering data.

It is sometimes contended that the Tassie (T), or hydrodynamical, model [16] is more appropriate for the transition density associated with excitation of a giant resonance that exhausts a large fraction of the sum-rule limit (but see Sec. III below). Indeed, the model (2.5) for the GMR is an example of this approach. Consequently we also made calculations using the Tassie model. In this we have

$$g_\ell^T(r)=-\alpha_\ell^m r^{\ell-1} d\rho(r)/dr \tag{2.7}$$

when $\ell\geq 2$, instead of the BM form (2.4). The additional factor of $r^{\ell-1}$ tends to shift the Tassie transition density to larger radii than the BM one and hence enhances the transition potential for the peripheral collisions that are important for heavy ions. This is compensated for in part if one demands that both transition models exhaust the same fraction of the sum-rule limit for the operator r^ℓ (see Sec. III below). This condition provides a relationship between the amplitudes δ_ℓ^m and α_ℓ^m for the two models. Define the transition multipole moment for $\ell\geq 2$ by

$$M_\ell^i=\int g_\ell^i(r) r^{\ell+2} dr, \tag{2.8a}$$

with $i=$ BM or T. Integration by parts immediately gives

$$M_\ell^{\rm BM}=(\ell+2)\delta_\ell^m(A/4\pi)\langle r^{\ell-1}\rangle_m \tag{2.9a}$$

and

$$M_\ell^T=(2\ell+1)\alpha_\ell^m(A/4\pi)\langle r^{2\ell-2}\rangle_m, \tag{2.9b}$$

where the radial averages $\langle r^n\rangle_m$ are taken over the ground-state matter distribution $\rho(r)$. Equating $M_\ell^T=M_\ell^{\rm BM}$ gives the desired relation:

$$\alpha_\ell^m=\delta_\ell^m\frac{(\ell+2)\langle r^{\ell-1}\rangle_m}{(2\ell+1)\langle r^{2\ell-2}\rangle_m}. \tag{2.10}$$

In the monopole case, $\ell=0$, we define the transition multipole moment for the operator r^2,

$$M_0=(4\pi)^{1/2}\int g_0(r) r^4 dr. \tag{2.8b}$$

This becomes

$$M_0=\alpha_0^m A\langle r^2\rangle_m/\pi^{1/2} \tag{2.9c}$$

if the transition density (2.5) is used.

We may also define an isoscalar transition rate,

$$B({\rm IS},\ell)=|M_\ell|^2. \tag{2.11}$$

For our present purpose of comparing folding and DP models, we assume that the transitions are purely "isoscalar." That is, we assume that the neutron and proton contributions to the density distribution, $\rho=\rho_n+\rho_p$, have the same shape so that

$$\rho_n(r)=(N/A)\rho(r),\quad \rho_p(r)=(Z/A)\rho(r). \tag{2.12}$$

The corresponding parts of the transition density, $g_\ell=g_{n\ell}+g_{p\ell}$, have the same property and hence their moments are also in the ratio

$$M_{n\ell}/M_{p\ell}=N/Z. \tag{2.13}$$

The associated electric transition rate is then

$$B(E\ell)\uparrow=(Z/A)^2B(\mathrm{IS},\ell)e^2. \tag{2.14}$$

C. Deformed potential model

The standard DP model [8] results in transition potentials whose shapes (in contrast to the folding procedure) are independent of multipolarity for $\ell\geq 2$:

$$G_\ell^{\mathrm{DP}}(r)=-\delta_\ell^U dU(r)/dr, \tag{2.15}$$

where δ_ℓ^U is the potential deformation length for the transition and $U(r)$ is the optical potential that reproduces the observed elastic scattering. We take the usual Woods-Saxon form for U, with the published [3–7] parameter values.

The DP model has also been applied to the excitation of the GMR, assuming this to be a breathing mode [18]. Then, by analogy with the transition density (2.5), we have

$$G_0^{\mathrm{DP}}(r)=-\alpha_0^U[3U(r)+rdU(r)/dr], \tag{2.16}$$

which has a node in the surface. This has been called "version 1" of the DP model for monopoles [18], and was used in Refs. [5,6]. However, a slightly different "version 2" [18] was used by the authors of Ref. [7].

We must relate the deformation length δ_ℓ^m or amplitude α_0^m for the matter distribution to those for the potential in order to compare the consequences of using folding or the DP model for a given transition. It has become conventional to equate the deformation lengths when $\ell\geq 2$,

$$\delta_\ell^U=\delta_\ell^m, \tag{2.17}$$

because this results in the same displacements of the surfaces of the potential and matter distribution. It is not at all clear how the monopole amplitudes should be related, but in the same spirit we equate the displacements at the corresponding potential or matter radius,

$$\alpha_0^U R_U=\alpha_0^m c, \tag{2.18}$$

where R_U is the radius of the Woods-Saxon potential and c is the matter radius in Eq. (2.6). The values of δ_ℓ^m and α_0^m are related to sum-rule limits in Sec. 3.

D. Coulomb excitation

The effects of Coulomb excitation are included by adding to the transition potential the almost model-independent term

$$G_\ell^C(r)=\pm 4\pi[B(E\ell)\uparrow]^{1/2}Z_p e/(2\ell+1)\times\begin{cases}1/r^{\ell+1}, & r\geq R_c\\ r^\ell/R_c^{2\ell+1}, & r\leq R_c\end{cases} \tag{2.19}$$

where $Z_p e$ is the charge on the projectile and $R_c=1.2(A_T^{1/3}+A_p^{1/3})$ fm. Care must be taken to choose the appropriate sign relative to the hadronic component [9]. The plus sign is correct for the models and isoscalar transitions considered here. The electric transition rate $B(E\ell)$ is assumed to be related by Eq. (2.14) to the isoscalar one.

III. SUM-RULE LIMITS

Certain linearly energy-weighted sum rules (EWSR's) for the operators $r^\ell Y_\ell(\theta,\phi)(\ell\geq 2)$ and $r^2(\ell=0)$ provide convenient measures of the strength of transitions to giant resonances [19]. These transitions exhaust large fractions of the sum-rule limits. The operators for $\ell\geq 2$ are the same as those for electric excitation. Hadronic excitation by inelastic scattering is associated with a different radial dependence, but the target nucleus surface is emphasized just as it is by the r^ℓ operator, and we can expect the sum-rule expressions to provide a qualitatively reliable guide [8].

If a single state with excitation energy E_x exhausts 100% of the isoscalar EWSR for $\ell\geq 2$, the transition rate is

$$B(\mathrm{IS},\ell)=\frac{\hbar^2}{2m}\frac{A}{4\pi E_x}\ell(2\ell+1)^2\langle r^{2\ell-2}\rangle_m. \tag{3.1}$$

This requires a deformation length for the BM model transition density (2.4) given by

$$(\delta_\ell^m)^2=\frac{\hbar^2}{2m}\frac{4\pi}{AE_x}\frac{\ell(2\ell+1)^2}{(\ell+2)^2}\frac{\langle r^{2\ell-2}\rangle_m}{\langle r^{\ell-1}\rangle_m^2}. \tag{3.2}$$

On the other hand, if the transition density has the Tassie form (2.7), we need

$$(\alpha_\ell^m)^2=\frac{\hbar^2}{2m}\frac{4\pi}{AE_x}\frac{\ell}{\langle r^{2\ell-2}\rangle_m}. \tag{3.3}$$

A monopole excitation that exhausts the sum rule has

$$B(\mathrm{IS},0)=\frac{\hbar^2}{2m}\frac{4A}{E_x}\langle r^2\rangle_m \tag{3.4}$$

and the transition density (2.5) requires an amplitude

$$(\alpha_0^m)^2=\frac{\hbar^2}{2m}\frac{4\pi}{AE_x}\frac{1}{\langle r^2\rangle_m}. \tag{3.5}$$

The above expressions are frequently approximated by assuming that the density distribution is uniform with a radius R, for which the radial averages become

$$\langle r^n\rangle_m=\frac{3R^n}{n+3}. \tag{3.6}$$

The value $R=1.20A^{1/3}$ fm is usually adopted. We prefer for consistency to use the actual averages appropriate for the model density distributions used in the folding calculations. These agree, for $\ell=0$ and 2, with the estimate (3.6) if a slightly larger radius R is used, $R=r_0A^{1/3}$, with $r_0\approx 1.21$ to 1.23. The deviations become larger as n increases.

The transition rates and amplitudes resulting from Eqs. (2.14) and (3.1)–(3.5) for 100% of the EWSR limit are listed in Tables I and II.

Sum-rule arguments have also been used [19] to show that, if a single excited state saturates the EWSR for r^ℓ, the associated radial transition density has the form

TABLE II. Sum-rule limits for giant monopole resonances with excitation energy E_x.

	E_x (MeV)	B(IS,0) (b^2)	α_0^m
^{60}Ni	19.4	0.354	0.128
^{90}Zr	16.4	0.829	0.099
^{118}Sn	15.5	1.397	0.081
^{120}Sn	15.7	1.415	0.079
^{124}Sn	15.3	1.532	0.078
^{208}Pb	13.9	3.853	0.054

$$g_\ell(r) = -\alpha_\ell^m r^{\ell-1} d\rho(r)/dr + \Delta g_\ell(r) \tag{3.7}$$

with α_ℓ^m given by Eq. (22). Here $\Delta g_\ell(r)$ is not determined, but must satisfy

$$\int \Delta g_\ell(r) r^{\ell+2} dr = 0. \tag{3.8}$$

This condition guarantees that Δg_ℓ does not contribute transition strength for the multipole operator with radial dependence r^ℓ. However, it may still contribute to the hadronic excitation operator which has a different radial dependence.

The first term on the right of Eq. (3.7) is just the Tassie form (2.7), and this has been used to argue that the T form is appropriate for the excitation of giant resonances which exhaust a large fraction of the EWSR limit. However, the possible presence of a Δg_ℓ term weakens this argument. Furthermore, the observed giant resonances are not single excited states but spread over several MeV of excitation, and usually substantial fractions of the EWSR strength limits are also observed elsewhere in the spectrum. Beyond these remarks, little can be said, except to note that nuclear structure calculations of the random-phase approximation (RPA) type appear consistently to predict transition densities for the excitation of giant resonances with $\ell \geq 2$ that are closer to the BM form than to the Tassie one [20].

IV. EXCITATION OF THE GQR BY ^{17}O AT $E/A = 84$ MeV

A. Comparison of models

Coulomb excitation is important for $\ell = 2$, and can be dominant for heavy (large $Z_p Z_T$) systems [1,2]. This tends to obscure differences in the hadronic component between the folding and DP approaches. Consequently, in each case we made calculations both with and without Coulomb excitation so as to see these differences more clearly and to judge their importance. The cross sections were calculated using relativistic kinematics in the coupled-channels program PTOLEMY [21], although it was confirmed that the distorted-wave Born approximation gave results that were almost indistinguishable. Initially, we assumed 100% depletion of the sum-rule limit (3.2) or (3.3), together with the relation (2.17) for the DP model. Later we adjusted the results to fit the measured cross sections and thus obtain a measure of the experimental depletion of the sum-rule limit.

Data are available [3–7] for the six targets ^{60}Ni, ^{90}Zr, ^{118,120,124}Sn, and ^{208}Pb. The density parameters we used and the corresponding sum rule quantities are listed in Table I.

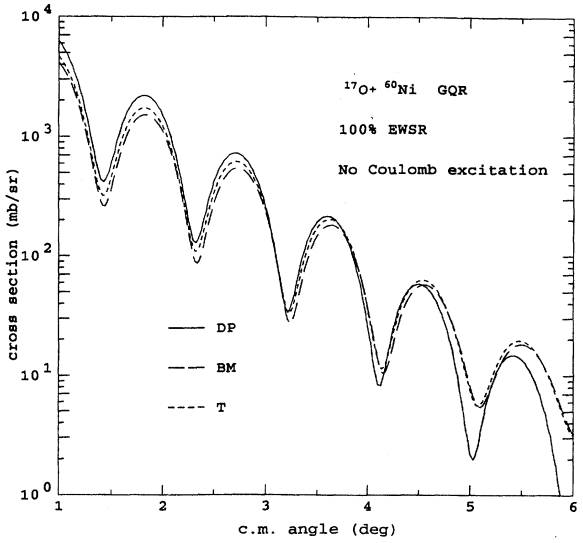

FIG. 1. Comparison of differential cross sections for ^{17}O ions with $E/A = 84$ MeV exciting a giant quadrupole resonance (GQR) in ^{60}Ni predicted by using the deformed potential (DP) model (solid curve) and by using folding with a Bohr-Mottelson (BM) transition density (long-dashed curve) or a Tassie (T) transition density (short-dashed curve). In each case, the strength is chosen to exhaust 100% of the energy-weighted sum-rule limit. No Coulomb excitation was included.

The sum-rule limit (3.2) for the deformation length involves the ratio $\langle r^2 \rangle_m / \langle r \rangle_m^2$. Equation (3.6) shows this to be 16/15 for a uniform distribution, independent of R. We find values only 2–3 % larger using the more realistic Fermi shapes.

First, we consider the cross sections calculated without Coulomb excitation; results for the two folding models (BM and T transition densities) are compared with those for the DP model in Figs. 1–4. (Results for the other two Sn isotopes are very similar to those for ^{120}Sn.) These are all for 100% of the sum-rule limit as defined by Eqs. (2.14), (2.17),

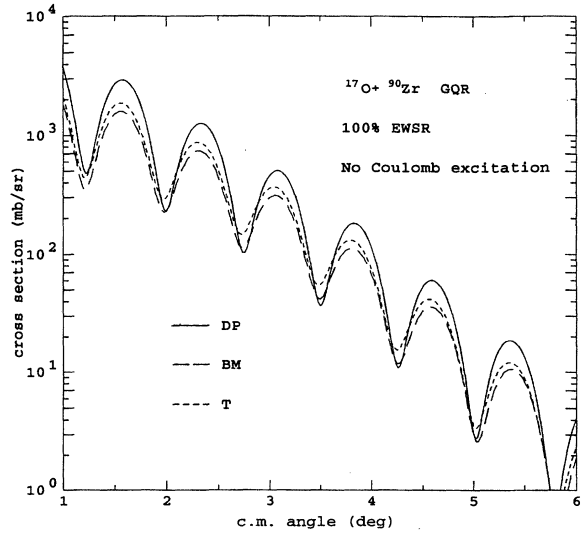

FIG. 2. As Fig. 1, except for ^{90}Zr.

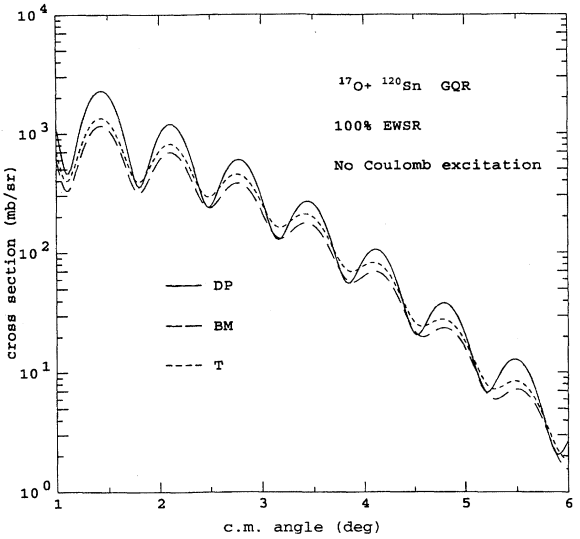

FIG. 3. As Fig. 1, except for ^{120}Sn.

and (3.1)–(3.3), and Table I. The BM and T models give very similar angular distributions, with the T cross sections being somewhat larger in magnitude by 10–20 %.

Comparing the folding and DP results suggests that folding results in less marked oscillations in the angular distributions, except for ^{60}Ni. However, closer examination reveals that this feature is somewhat dependent on the properties of the Woods-Saxon potentials used for the DP model. In particular, it is correlated with the ratio of imaginary to real potential strengths. Except for ^{60}Ni, the Woods-Saxon potentials [3–7] have W/V ratios that are smaller than w/v [14] for the folding interaction by about 30%, even though the corresponding fits to the elastic scattering data are similar in quality. This point is emphasized for ^{208}Pb if the Woods-Saxon from Ref. [3] is used in the DP model instead of that from Ref. [7]. The W/V ratio from Ref. [3] equals the

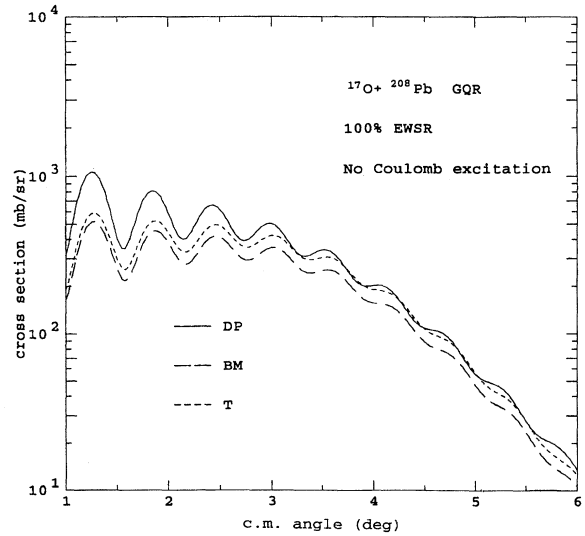

FIG. 4. As Fig. 1, except for ^{208}Pb.

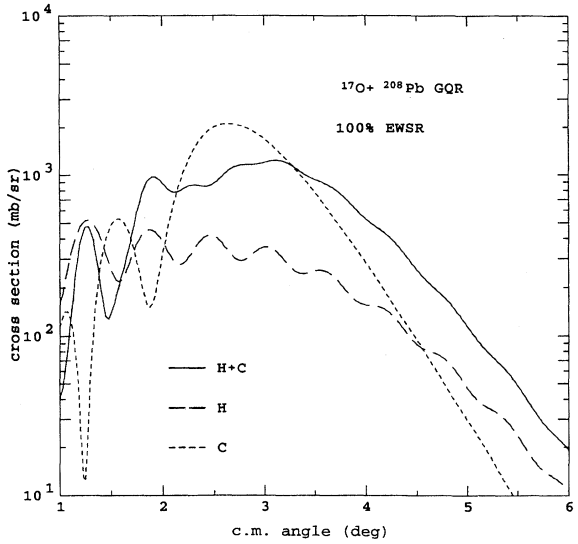

FIG. 5. Predictions for exciting the GQR in ^{208}Pb using the folding model with the BM transition density and exhausting 100% of the sum-rule limit. The short-dashed curve is for Coulomb excitation alone, the long-dashed curve is for the hadronic interaction alone, while the solid curve is for their coherent sum. The relative Coulomb and hadronic strengths assume a purely isoscalar transition, $B(E2)=(Ze/A)^2B(\mathrm{IS},2)$.

w/v ratio of the folding interaction, and the corresponding angular distributions are almost identical.

The Coulomb-hadronic interference that occurs when Coulomb excitation is included may alter the angular distribution drastically, especially for the heavy targets (large Z_T). The effect on the ^{60}Ni excitation is rather small and consists mainly in making the minima more shallow at small angles. On the other hand, the Coulomb excitation dominates the cross section for ^{208}Pb [3,7]. Figure 5 shows the cross sections for hadronic or Coulomb excitation alone and their combined effect. However, the hadronic interaction is not negligible; even here as Fig. 5 shows, it changes the angular distribution radically. The result in this case is not extremely sensitive to the hadronic component; in one sense, this is fortunate because it allows us to extract a $B(E2)$ value that is almost model independent. In another sense, it is unfortunate because it requires very precise data in order to determine any detailed characteristics of the hadronic interaction other than its overall strength. [Nonetheless, the sensitivity is sufficient to rule out definitively the $B(E2)$ and $B(\mathrm{IS},2)$ values deduced from (π,π') measurements on the GQR excitation in ^{208}Pb [12].]

Another feature of Coulomb excitation to which attention should be drawn is its sensitivity to the excitation energy. This is relevant because giant resonances may have widths of several MeV. The Coulomb excitation probability may vary significantly over this energy range, and the cross section should be integrated across the resonance. For example, in the present case a decrease of 2 MeV in E_x for the GQR in ^{208}Pb increases the Coulomb cross section by 30%. This effect is important for excitation of the broad giant dipole resonance [4] ($\Gamma\sim4$ MeV), but much less so for the narrower

TABLE III. Ratios of integrated cross sections σ_t for ^{17}O at $E/A=84$ MeV for a given fraction of the sum-rule limit. DP refers to the deformed potential, BM to Bohr-Mottelson, and T to Tassie.

Target	^{60}Ni	^{90}Zr	^{118}Sn	^{120}Sn	^{124}Sn	^{208}Pb
GQR						
Hadronic only						
$\sigma_t(T)/\sigma_t$(BM)	1.13	1.18	1.15	1.17	1.17	1.18
σ_t(DP)/σ_t(BM)	1.42	1.81	1.72	1.71	1.41	1.50 (1.18) [a]
Hadronic + Coul. ex.						
$\sigma_t(T)/\sigma_t$(BM)	1.11	1.11	1.06	1.08	1.08	1.03
σ_t(DP)/σ_t(BM)	1.37	1.52	1.32	1.31	1.20	1.09 (1.02) [a]
GMR						
σ_t(DP)/$\sigma_t(T)$	1.26	1.55	1.68	1.69	1.40	1.51 (1.21) [a]

[a]Values in parentheses result from using in the DP calculations the Woods-Saxon potential from Ref. [3], instead of that from Ref. [7].

GQR ($\Gamma\sim2$ MeV). We simply used the peak E_x values given in Table I.

The integrated cross sections

$$\sigma_t=\int_{4\pi}\frac{d\sigma(\theta)}{d\omega}\,d\omega \tag{4.1}$$

give a measure of the relative magnitudes of the cross sections obtained using the various models, though it should be remembered that the differential cross sections at a given angle, such as at a forward peak where theoretical curves are frequently normalized to measured cross sections, may exhibit somewhat different ratios because of differences in the angular distributions.

Ratios of the various integrated cross sections for the same fraction of the sum rule limit are collected in Table III. Values both with and without the inclusion of Coulomb excitation are considered. Without Coulomb excitation, use of the Tassie (T) transition density results in cross sections that are 13% to 18% larger than when the BM transition density is used. The deformed potential (DP) procedure gives even larger cross sections than the BM model, just as was found for the excitation of low states [11]. These differences are ameliorated somewhat when Coulomb excitation is included, but still remain very significant except for ^{208}Pb where the Coulomb excitation dominates.

B. Comparison with measured cross sections

Now we compare the calculated (including Coulomb excitation) and measured cross sections and attempt to deduce what fraction of the sum-rule limit has been observed. Two points have to be kept in mind here. First, no account has been taken of the variation of the Coulomb excitation as the excitation energy varies over the resonance; calculations were only made for the peak value of E_x as given in Table I. Secondly, the theoretical curves were not averaged to account for the finite angular resolution of the measurements; this will tend to make the observed minima less sharp than the theoretical ones and to slightly flatten the maxima. Furthermore, there are subjective uncertainties in the way we choose to normalize the theoretical curves to the data. However, our main purpose here is to compare the *relative* results of using folding versus the DP model.

No attempt was made to optimize the fits by adjusting the value (2.14) assumed for the ratio $B(E2)\uparrow/B(\mathrm{IS},2)$, which could alter the Coulomb-hadronic interference pattern. That is, all the calculations presented are for pure "isoscalar" ($M_n/M_p=N/Z$) transitions. It will be seen that this assumption gives an adequate description of the data. It has been demonstrated elsewhere [4–6,12] that departures from this ratio as large as those inferred from (π,π') measurements are incompatible with the heavy-ion data.

Comparisons with the measured cross sections are presented in Figs. 6–11 and the corresponding percentages of the sum-rule limits used for the theoretical curves are given in Table IV. Uncertainties of at least ±10 should be ascribed to these percentages. Only the folding model results using

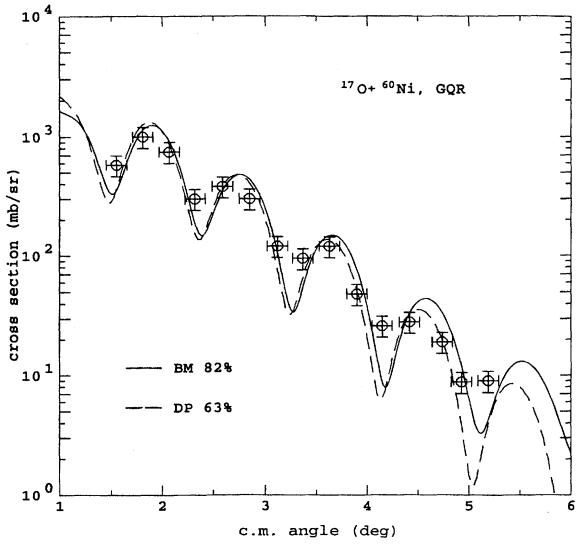

FIG. 6. Predictions from the folding model with the BM transition density (solid curve) and the DP model (dashed curve) compared with the measured cross sections for ^{17}O ions with $E/A=84$ MeV exciting the GQR in ^{60}Ni. The percentages of the sum-rule limit used are indicated. Coulomb excitation was included, assuming a purely isoscalar transition. The data are from Ref. [7].

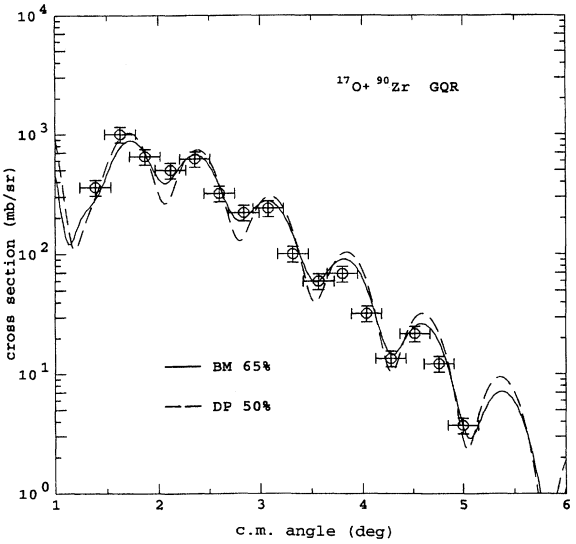

FIG. 7. As Fig. 6, except for ^{90}Zr.

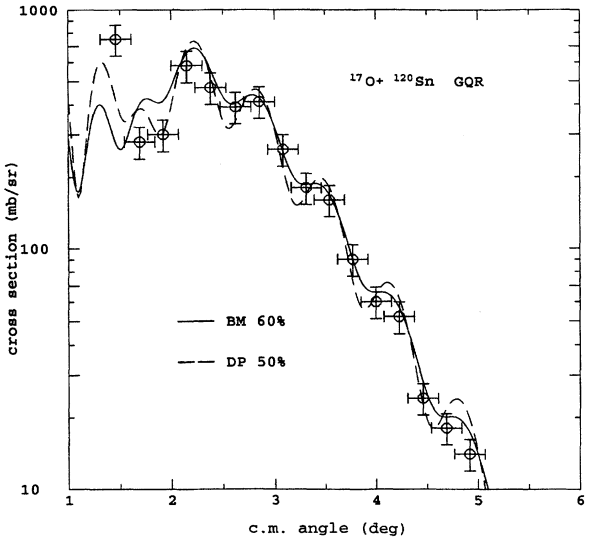

FIG. 9. As Fig. 6, except for ^{120}Sn.

the BM transition densities (4) are shown in the figures because the Tassie form (7) gives almost identical angular distributions but, except for ^{208}Pb, requires about 10% less of the sum-rule limit. The DP curve for ^{208}Pb was obtained using the optical potential from Ref. [7]; use of the potential from Ref. [3] gives results even closer to those from folding.

Overall, the use of folding with the BM transition densities leads one to infer (except for ^{208}Pb) some 10–20% more depletion of the EWSR limit than when analyzing the data using the DP model. The ^{208}Pb excitation is so dominated by Coulomb excitation that it is less sensitive to the precise strength of the hadronic component and equally good fits to the data (Fig. 11) can be obtained with either model exhausting 55% of the sum-rule limit. The results for the other targets are of the same order as (although somewhat less than) what one would expect from the ratios of integrated cross sections given in Table III. They are not the same because differences in the angular distributions affect how one chooses to fit to the data.

The BM model for the transition densities, although somewhat arbitrary, is a natural choice for comparison with the DP model because the same kind of physical assumptions are made in both models. Use of the T model densities provides some measure of the sensitivity of the folding procedure to the form of the transition density. They provide angular distributions that are very similar to the BM ones but with cross sections (again, except for ^{208}Pb) that are about 10% larger.

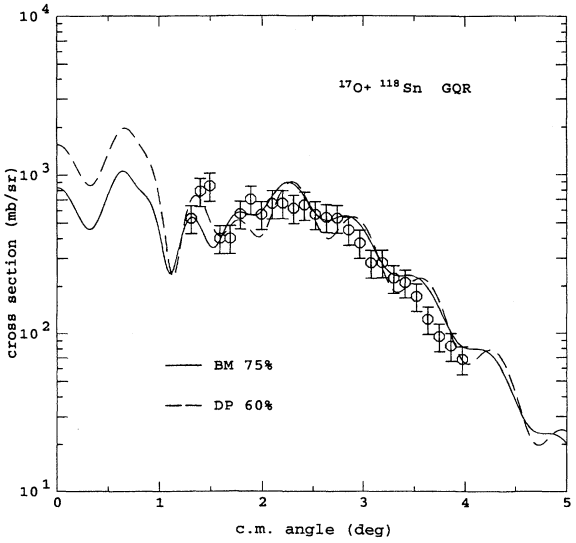

FIG. 8. As Fig. 6, except for ^{118}Sn. Here the data are from Ref. [5].

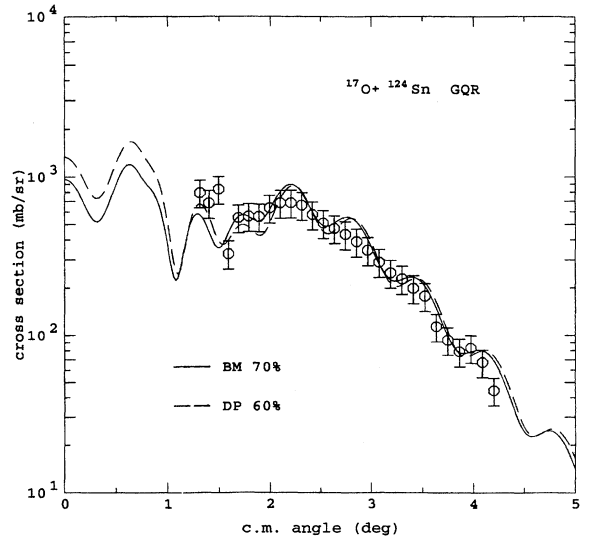

FIG. 10. As Fig. 6, except for ^{124}Sn. Here the data are from Ref. [6].

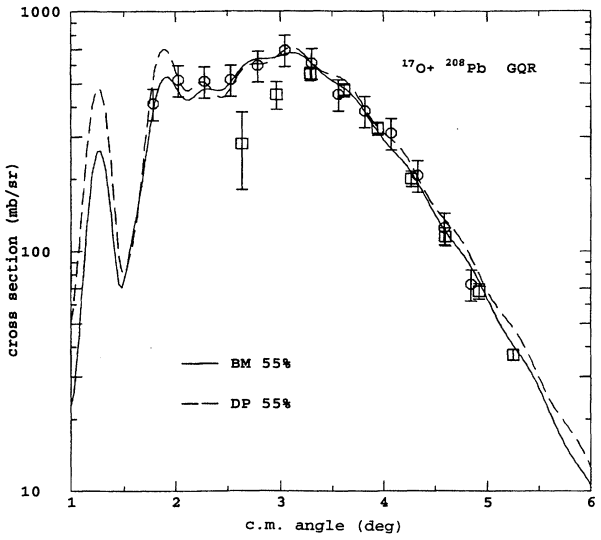

FIG. 11. As Fig. 6, except for ^{208}Pb. The circles are data from Ref. [4]; the squares are data from Ref. [7].

V. EXCITATION OF THE GMR BY ^{17}O AT $E/A = 84$ MeV

A. Comparison of models

It has been emphasized many times (see [11] for a recent example) that the transition potentials generated by the folding model differ considerably in shape from those of the DP model. The differences are particularly marked in the case of the monopole breathing mode excitation. Figure 12 compares them for the ^{60}Ni target. The folding was done using the Tassie transition density (2.5), while the DP transition potential is given by (2.16) with the scaling relation (2.18). Both are normalized to correspond to 100% of the EWSR limit (3.5). The transition potentials for other targets are similar; all have a node in the surface, with that for the DP model occurring at a radius larger by 1.5 to 2 fm than that for folding. The values in the interior are very different but become rather similar at the large radii which are encountered in peripheral collisions. (For example, the strong absorption radius for ^{17}O+ ^{60}Ni is about 8 fm, while that for ^{17}O+ ^{208}Pb is approximately 10.5 fm.)

Figures 13 to 18 compare the differential cross sections predicted by the two models, each corresponding to 100% saturation of the sum-rule limit. The oscillatory angular distributions are rather similar except for a tendency of the folding approach to give less deep minima. Overall, the DP model yields peak cross sections that are from 25% to 70% larger than those from folding. Another measure of the differences in magnitude is given by the ratios of the integrated cross sections (4.1) for the two models. These are included in Table III and closely follow the ratios of peak cross sections.

Some uncertainties were explored for ^{17}O+ ^{208}Pb. For example, if the Woods-Saxon potential from [3] is used in the DP model instead of that from [7], the predicted cross sections (shown by the short-dashed curve in Fig. 18) are reduced by 20%, bringing them closer to the folding model results.

TABLE IV. Percentages of sum-rule limits used in constructing the theoretical fits to the data shown in Figs. 6–11 for excitation of the GQR.

Target	^{60}Ni	^{90}Zr	^{118}Sn	^{120}Sn	^{124}Sn	^{208}Pb
DP [a]	63	50	60	50	60	55
BM	82	65	75	60	70	55
T [b]	74	59	70	55	65	55

[a]Except for ^{208}Pb, the DP values used were taken from the corresponding experimental papers [5–7].

[b]Curves not shown in Figs. 6–11 because they are very close to the BM ones.

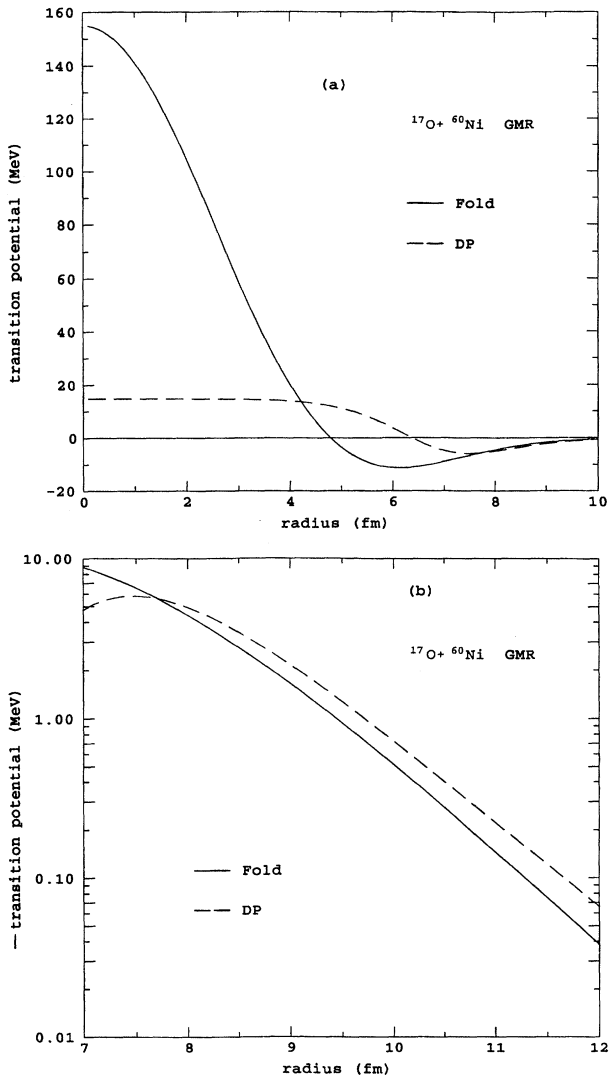

FIG. 12. Comparison of transition potentials for ^{17}O ions exciting the giant monopole resonance (GMR) in ^{60}Ni. Solid curve: folding model using the Tassie transition density; dashed curve: deformed potential model, version 1. Both are normalized to exhaust 100% of the energy-weighted sum-rule limit. The strong absorption radius for this system at $E/A = 84$ MeV is approximately 8 fm.

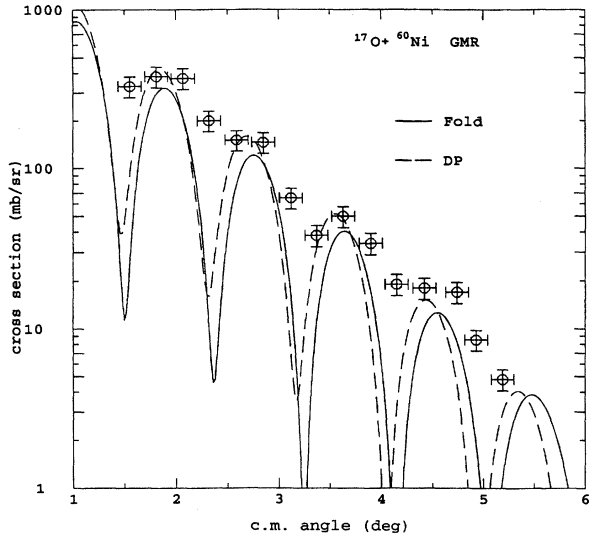

FIG. 13. Predicted differential cross sections for 100% of the sum rule limit for ^{17}O ions with $E/A = 84$ MeV exciting the GMR in ^{60}Ni, compared with cross sections extracted from measurements [7]. Solid curve: folding model; dashed curve: deformed potential model.

Another uncertainty concerns the form chosen for the transition density in folding or the transition potential in the DP model. Use of a slightly different "version 2" [18] (used for the DP model in Ref. [7]) results in cross sections that are 10% (DP) or 15% (folding) smaller than given by version 1 of (2.5) and (2.16). We also generated a transition density for the GMR from a simple RPA model [20]. The resulting transition potential and differential cross sections were very similar to that obtained using the version 1 model (2.5).

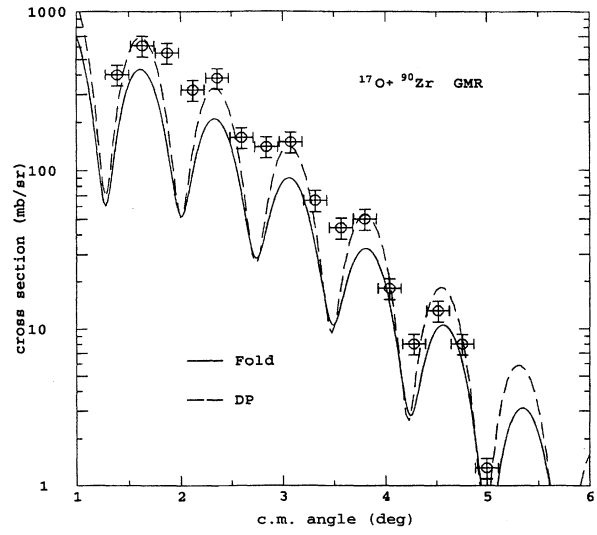

FIG. 14. As Fig. 13, except for ^{90}Zr.

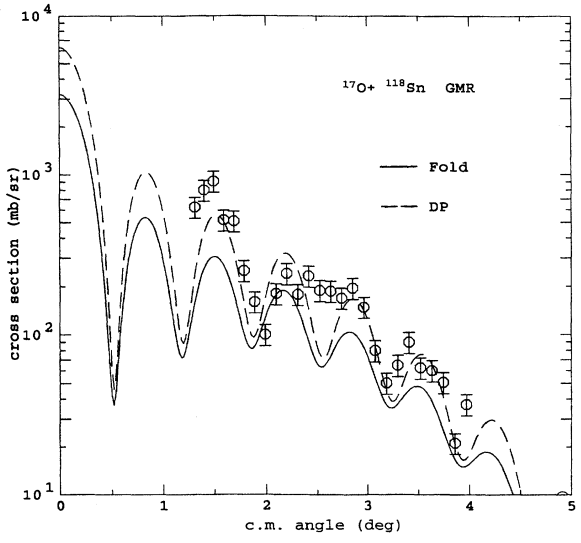

FIG. 15. As Fig. 13, except for ^{118}Sn. Here the data are from Ref. [5].

B. Comparison with measured cross sections

The differential cross sections for the GMR deduced from measurements [3–7] are included in Figs. 13–18. The theoretical curves shown were not averaged to account for the finite angular resolution of the measurements. Such averaging can be important for the sharp oscillations predicted for a monopole excitation.

It is clear that the data exceed the predictions for 100% saturation of the sum-rule limit for either the DP or the folding model. The measurements imply strengths ranging from 120% to 135% of the EWSR limit when the DP model is used, as was found previously [4–7]. The more forward-angle data for ^{208}Pb from Ref. [4] indicate an even larger discrepancy of about a factor of 2. The situation is worse for

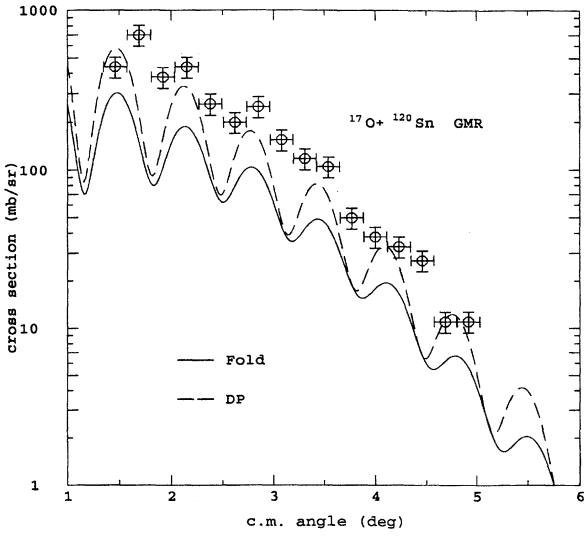

FIG. 16. As Fig. 13, except for ^{120}Sn.

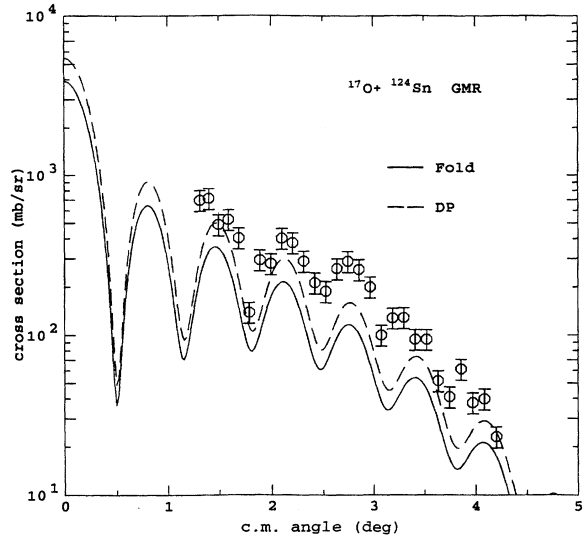

FIG. 17. As Fig. 13, except for ^{124}Sn. Here the data are from Ref. [6].

the folding model, which we believe to be more "realistic." Strengths close to twice the sum-rule limit (even more for the data of Ref. [4]) are needed to fit the data.

This is not without precedent. An analogous study of the giant monopole resonance excitation by 152 MeV α particles [22] gave similar results: folding gave appreciably smaller cross sections than given by the DP model, and the data implied strengths exceeding the sum rule limits.

It is possible that the simple Tassie form (2.5) is inadequate, although several RPA calculations have resulted in transition densities that are very similar to this form. At one time, it was thought [9] that neglect of density dependence in the effective interaction might be responsible for the GMR discrepancies, but explicit calculations [23] indicated that it was not. Perhaps a more plausible explanation is the presence of contributions in the spectra from other ℓ values. A popular candidate is a fragment of a giant hexadecapole ($\ell=4$) resonance. It is known [7], for example, that a small fraction of the sum-rule limit for $\ell = 4$ (15% for ^{208}Pb, 10% for ^{90}Zr) will produce cross sections as large as those for 100% of the GMR.

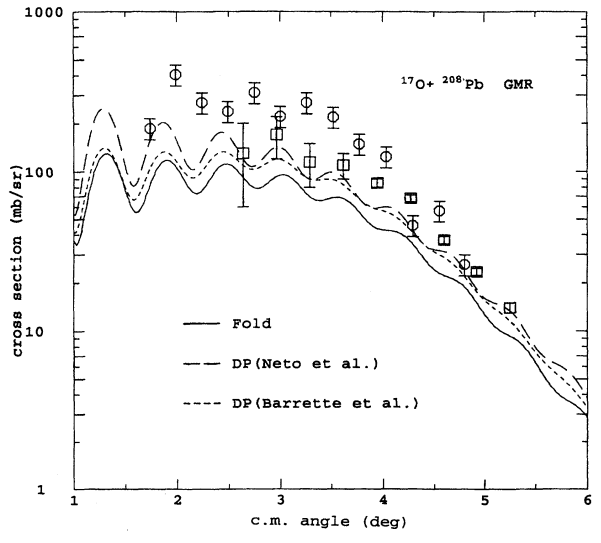

FIG. 18. As Fig. 13, except for ^{208}Pb. The long-dashed DP curve is based upon the optical potential from Ref. [7], while the short-dashed curve uses the potential from Ref. [3]. The circles are data from Ref. [3], the squares from Ref. [7].

VI. SUMMARY AND DISCUSSION

We contend that the use of folded potentials to analyze scattering measurements is more meaningful than employing the deformed optical potential (DP) model because folding provides a direct link to the underlying transition density of the target nucleus, whereas the DP model has no such basis. It is the properties of the transition density about which we wish to learn. The two approaches can lead to significantly different results. In this work, we have investigated these differences for the analysis of excitations of giant monopole (GMR) and quadrupole (GQR) resonances by heavy-ion scattering, in particular as induced by ^{17}O beams at $E/A = 84$ MeV.

Overall, the effects we find are certainly not negligible. The measures we obtain for the percentages of the EWSR limits for the GQR that are needed to fit the data are increased by 10–20% (except for ^{208}Pb, where Coulomb excitation dominates) when folding is used. However, all the data remain compatible with the assumption that the transitions are purely isoscalar. The disagreements with the interpretation of inelastic pion scattering data remain.

Similar differences are found for excitation of the GMR. Use of the DP model already shows a need for more than 100% of the EWSR limit (typically ~125%, except possibly for ^{208}Pb where the cross sections at the smaller angles reported in [4] imply nearly twice the sum-rule limit). This situation is exacerbated when folding is used and strengths close to, or even greater than, twice the sum-rule limit are needed to fit the data. This may be due to deficiencies in the simple Tassie model of the transition density that we have used, although several nuclear structure calculations lend support to this form. An alternative suggestion is that the presence in the extracted cross sections of a "background" of excitations with other multipolarities, especially $\ell=4$, is responsible for the discrepancies. An $\ell=4$ excitation with a strength of only 10–15 % of the hexadecapole sum rule limit has cross sections comparable to 100% of the monopole.

Our studies have concentrated on excitations by ^{17}O ions with $E/A = 84$ MeV because the most complete data are available for this beam. However, the same qualitative features are expected for other heavy ions and other energies. The differences between using folding and the DP model tend to be reduced as the energy is lowered. On the other hand, the effects on the hadronic amplitude become larger as the mass (size) of the projectile is increased. In particular, the differences between DP and folding models increase more

rapidly with multipolarity. However, a larger mass usually means also a larger charge and the importance of Coulomb excitation is enhanced.

Finally, it must be stressed that the differences between the results of applying the DP and folding approaches increase strongly as the multipolarity ℓ increases. This situation will be discussed elsewhere.

ACKNOWLEDGMENTS

We are indebted to P. Roussel-Chomaz and N. Alamanos for providing numerical listings of their data [7]. This research was sponsored by the Division of Nuclear Physics, U.S. Department of Energy under Contract No. DE-AC05-84OR21400 managed by Martin Marietta Energy Systems, Inc.

[1] F. E. Bertrand, J. R. Beene, and D. J. Horen, Nucl. Phys. **A482**, 287c (1988); **A488**, 163c (1988); J. R. Beene and F. E. Bertrand, *ibid.* **A538**, 553c (1992).

[2] J. R. Beene, Nucl. Phys. **A569**, 163c (1994).

[3] J. Barrette, N. Alamanos, F. Auger, B. Fernandez, A. Gillibert, D. J. Horen, J. R. Beene, F. E. Bertrand, R. L. Auble, B. L. Burks, J. Gomez del Campo, M. L. Halbert, R. O. Sayer, W. Mittig, Y. Schutz, B. Haas, and J. P. Vivien, Phys. Lett. B **209**, 182 (1988).

[4] J. R. Beene, F. E. Bertrand, D. J. Horen, R. L. Auble, B. L. Burks, J. Gomez del Campo, M. L. Halbert, R. O. Sayer, W. Mittig, Y. Schutz, J. Barrette, N. Alamanos, F. Auger, B. Fernandez, A. Gillibert, B. Haas, and J. P. Vivien, Phys. Rev. C **41**, 920 (1990).

[5] D. J. Horen, F. E. Bertrand, J. R. Beene, G. R. Satchler, W. Mittig, A. C. C. Villari, Y. Schutz, Zhen Wenlong, E. Plagnol, and A. Gillibert, Phys. Rev. C **42**, 2412 (1990).

[6] D. J. Horen, F. E. Bertrand, J. R. Beene, G. R. Satchler, W. Mittig, A. C. C. Villari, Y. Schutz, Zhen Wenlong, E. Plagnol, and A. Gillibert, Phys. Rev. C **44**, 2385 (1991).

[7] R. Liguori Neto, P. Roussel-Chomaz, L. Rochais, N. Alamanos, F. Auger, B. Fernandez, J. Gastebois, A. Gillibert, R. Lacey, A. Miczaika, D. Pierroutsakou, J. Barrette, S. K. Mark, R. Turcote, Y. Blumenfeld, N. Frascaria, J. P. Garron, J. C. Roynette, J. A. Scarpaci, T. Suomijarvi, A. Van der Woude, and A. M. Van den Berg, Nucl. Phys. **A560**, 733 (1993).

[8] G. R. Satchler, *Direct Nuclear Reactions* (Oxford University Press, Oxford, 1983).

[9] G. R. Satchler, Nucl. Phys. **A472**, 215 (1987).

[10] J. R. Beene, D. J. Horen, and G. R. Satchler, Phys. Rev. C **48**, 3128 (1993).

[11] J. R. Beene, D. J. Horen, and G. R. Satchler, Phys. Lett. B **344**, 67 (1995).

[12] D. J. Horen, J. R. Beene, and F. E. Bertrand, Phys. Rev. C **37**, 888 (1988).

[13] G. R. Satchler and W. G. Love, Phys. Rep. **55**, 183 (1979), App. B.

[14] G. R. Satchler, Nucl. Phys. **A579**, 241 (1994).

[15] D. J. Horen, J. R. Beene, and G. R. Satchler, Phys. Lett. B **316**, 463 (1993).

[16] A. Bohr and B. R. Mottelson, *Nuclear Structure* (Benjamin, New York, 1975), Vol. 2.

[17] H. Uberall, *Electron Scattering from Complex Nuclei* (Academic Press, New York, 1971), Vol. B.

[18] G. R. Satchler, Part. Nucl. **5**, 105 (1973).

[19] H. Ui and T. Tsukamoto, Prog. Theor. Phys. **51**, 1377 (1974); E. Lipparini and S. Stringari, Phys. Rep. **175**, 103 (1989).

[20] J. Wambach (private communication).

[21] M. J. Rhoades-Brown, M. H. Macfarlane, and S. C. Pieper, Phys. Rev. C **21**, 2417 (1980); **21**, 2436 (1980).

[22] F. E. Bertrand, G. R. Satchler, D. J. Horen, J. R. Wu, A. D. Bacher, G. T. Emery, W. P. Jones, D.W. Miller, and A. van der Woude, Phys. Rev. C **22**, 1832 (1980).

[23] M. El-Azab Farid and G. R. Satchler, Nucl. Phys. **A481**, 542 (1988).